



## Aircraft Engineering and Aerospace Technology: An International Journal

Edge clutter rejection for PPI radar images

Weishi Chen Huansheng Ning

### Article information:

To cite this document:

Weishi Chen Huansheng Ning , (2013),"Edge clutter rejection for PPI radar images", Aircraft Engineering and Aerospace Technology: An International Journal, Vol. 86 Iss 1 pp. 19 - 25

Permanent link to this document:

<http://dx.doi.org/10.1108/AEAT-05-2012-0063>

Downloaded on: 07 July 2016, At: 00:49 (PT)

References: this document contains references to 12 other documents.

To copy this document: [permissions@emeraldinsight.com](mailto:permissions@emeraldinsight.com)

The fulltext of this document has been downloaded 107 times since 2013\*

### Users who downloaded this article also downloaded:

(2013),"Multiple-hypothesis RAIM algorithm with an RRAIM concept", Aircraft Engineering and Aerospace Technology, Vol. 86 Iss 1 pp. 26-32 <http://dx.doi.org/10.1108/AEAT-08-2012-0131>

(2013),"Effects of adding strip flap on a plunging airfoil", Aircraft Engineering and Aerospace Technology, Vol. 86 Iss 1 pp. 6-18 <http://dx.doi.org/10.1108/AEAT-08-2012-0129>

(2013),"Multibody analyses for performance and aeromechanics of a rotor in low-speed flight", Aircraft Engineering and Aerospace Technology, Vol. 86 Iss 1 pp. 33-42 <http://dx.doi.org/10.1108/AEAT-09-2012-0150>

Access to this document was granted through an Emerald subscription provided by emerald-srm:549559 []

### For Authors

If you would like to write for this, or any other Emerald publication, then please use our Emerald for Authors service information about how to choose which publication to write for and submission guidelines are available for all. Please visit [www.emeraldinsight.com/authors](http://www.emeraldinsight.com/authors) for more information.

### About Emerald [www.emeraldinsight.com](http://www.emeraldinsight.com)

Emerald is a global publisher linking research and practice to the benefit of society. The company manages a portfolio of more than 290 journals and over 2,350 books and book series volumes, as well as providing an extensive range of online products and additional customer resources and services.

Emerald is both COUNTER 4 and TRANSFER compliant. The organization is a partner of the Committee on Publication Ethics (COPE) and also works with Portico and the LOCKSS initiative for digital archive preservation.

\*Related content and download information correct at time of download.

# Edge clutter rejection for PPI radar images

Wei Shi Chen

China Academy of Civil Aviation Science and Technology, Beihang University, Beijing, China, and

Huansheng Ning

School of Electronics and Information Engineering, Beihang University, Beijing, China

## Abstract

**Purpose** – Incoherent primary radar is an applicable means for security surveillance of low-altitude airspace. An experimental airspace surveillance radar system has been developed for such applications. Target detector based on radar images is a powerful technique for the system. The main difficulty in designing such a detector is the rejection of heavy edge clutter for the plane position indicator (PPI) radar images after background subtraction.

**Design/methodology/approach** – The paper proposes an edge clutter rejection (ECR) detector with spatial characteristics to detect target instead of sheer threshold segmentation.

**Findings** – The paper chooses the optimal parameter values for the ECR detector and compares it with the existing techniques. Detection results show that the proposed detector achieves higher probability of detection with low false alarm rate, outperforming the fixed-threshold detector and the popular constant false alarm rate detectors. The ECR detector also presents limited computational cost due to its concentration on the pixels detected by the fixed-threshold algorithm with low threshold.

**Practical implications** – The aviation security of low-altitude airspace can be greatly increased by designing affordable airspace surveillance radar system.

**Originality/value** – The paper presents critical techniques for clutter rejection with PPI images, which is a significant part of the surveillance system.

**Keywords** Surveillance, CFAR, Clutter rejection, False alarm rate, Incoherent primary radar

**Paper type** Research paper

## Introduction

Generally, low-altitude airspace is the weak component of aviation safety surveillance and defense due to its limitation in technology and equipment. With the development of general aviation industry, safety monitor for low-altitude airspace has become a significant task of air defense system, in order to ensure safety of important regions and sensitive targets, such as border and coastal areas, towns or cities with concentrated population, high-rise buildings and busy airports (Lv *et al.*, 2009). Incoherent primary radar, which measures the azimuths and ranges of targets by detecting their echo signals, is a technical approach for security surveillance of low-altitude airspace, due to its low cost, easy installation and independent working ability. Digital plane position indicator (PPI) images are always collected by a capture card for the low-altitude surveillance radar system and processed by automatic multi-target recognition techniques. Because the monitoring region is low-altitude airspace with sophisticated background and heavy clutter while the interesting target is usually small aircraft with low radar cross-section, adaptive thresholding method should be used.

How to effectively and timely distinguish targets from strong clutter environment has been widely studied

(Vicen-Bueno *et al.*, 2009). The main objective of these studies is the separation of target and clutter with a fixed or adaptive threshold. A successful thresholding technique considers each pixel in a more adaptive environment (e.g. local neighborhood). The most popular adaptive detection techniques are the constant false alarm rate (CFAR) processors, which includes several improved processors such as the well-known cell averaging (CA) CFAR processor, the greatest of (GO) CFAR processor, the smallest of (SO) CFAR processor and the ordered statistics (OS) CFAR (He *et al.*, 2006). All these CFAR schemes set the threshold adaptively using estimated noise power by processing the reference cells surrounding the cell under investigation (Gandhi *et al.*, 1988). Hammoudi and Soltani (2004) improved the CA-CFAR and OS-CFAR detectors using fuzzy fusion rules in homogeneous and non-homogeneous backgrounds. Non-linear techniques based on artificial neural networks have been used these years. The ship detection in sea clutter could be solved by multilayer perceptrons (MLPs) without any prior knowledge of the statistical distributions (Vicen-Bueno *et al.*, 2011). Furthermore, targets mapped in images are always grey spots with high congregated degree, whereas, the clutters are independently distributed with lower congregated degree. This spatial characteristic was used in Li *et al.* (2009) to detect dim targets in a heavy clutter environment.

However, little study has been reported on specific techniques for target detection in low-altitude airspace from

The current issue and full text archive of this journal is available at [www.emeraldinsight.com/1748-8842.htm](http://www.emeraldinsight.com/1748-8842.htm)



Aircraft Engineering and Aerospace Technology: An International Journal  
86/1 (2014) 19–25  
© Emerald Group Publishing Limited [ISSN 1748-8842]  
[DOI 10.1108/AEAT-05-2012-0063]

This work is jointly funded by the National Natural Science Foundation of China (NSFC) and Civil Aviation Administration of China (CAAC) (61079019).

the PPI radar images, which is the subject of this paper. The PPI radar images were collected by our in-house airspace surveillance radar system. Due to the vertical coverage width of the radar beam, most of the echoes mapped in low-altitude PPI radar images are caused by objects on the ground (e.g. trees and buildings, etc.). Therefore, background subtraction is necessary. It should be noted that the edged echoes of the stationary background objects vary in continuous frames of the sequence, so the background information cannot be totally suppressed by background subtraction, leading to the serious inference of the edge background clutters. We propose an edge clutter rejection (ECR) detector with spatial characteristics instead of classical thresholding, leading to much easier rejection of the edged clutters.

The remainder of this paper is organized as follows. The second section introduces the data processing scheme of Beihang experimental airspace surveillance radar (BH-ASR). The third section, the details of the proposed clutter rejection method based on spatial characteristics are described, and several comparative algorithms are presented as references. The experimental results against ground-truth data are provided in the fourth section to demonstrate the performance of the proposed algorithm. Finally, some conclusions close the paper.

### Beihang experimental airspace surveillance radar

BH-ASR is a platform with further improvements based on the BHU avian radar experimental system (Ning *et al.*, 2010). The system has been tested at Shahe Reservoir, Beijing, and Nanyang Airport, Henan Province, central China. The out-field experiment is shown in Figure 1(a). We use X-band marine radar (Model 1941 Mark-2) as the sensor, whose working frequency is 9,410 MHz. Original PPI radar images (O) is collected by the capture card every 2.5 s and processed by the in-house data processing scheme shown in Figure 1(b).

The data processing scheme consists of three steps of background subtraction, clutter rejection and measurement extraction. Background subtraction is the first step in target detection, so it is essential to construct an adaptive background image. Since the background changes with time

due to the variations of the surrounding environment, the background image is usually updated as a time averaged version of the input image sequence periodically for engineering applications. After background subtraction, there is still a large quantity of clutter in the foreground image (F), especially distributed around the edge of the background objects, say edged clutter in this paper, so further clutter rejection is necessary. Generally, threshold calculation is the basic step for clutter suppression, since if the thresholds are too high, no targets will be seen. If the thresholds are too low, the system will be swamped with false alarms from clutter. In this paper, instead of merely depending on pixel intensity information from **F**, spatial distribution information from **O** is adopted for clutter rejection which will be discussed in detail in clutter rejection with spatial characteristics, named as the ECR detector. Then, the target pixels are labeled with 1 and the others with 0 in the binary image (**B**). In the third step, every connected area labeled 1 in **B** is considered as a measurement, whereas the center coordinates of these areas are extracted. Finally, the measurements are plotted on a satellite map or coordinate system in real time, and recorded to a database for further analysis.

### Clutter rejection technique for PPI radar images

Detection of low-altitude targets in PPI radar images is a challenge for incoherent primary radar due to the interference of edged clutters, whose intensities are sometimes even stronger than the real targets. Traditional segmentation method is commonly used with low detection threshold to increase the sensitivity of radar but the false alarm rate also increases as an unwanted side effect, so effective tracking approach is necessary to mitigate this effect at the cost of high computation load. In this section, we consider the spatial information in PPI images and propose an ECR detector, which is the main contribution of this paper. Then, several comparative algorithms are presented.

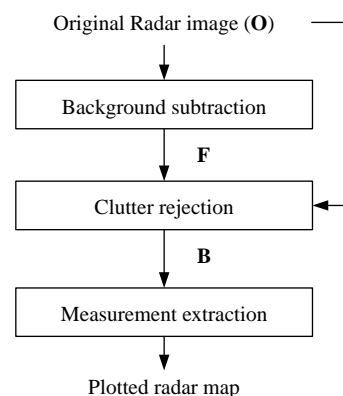
### Clutter rejection with spatial characteristics

To detect target in a PPI radar image, background information is subtracted from raw data first. However, after background subtraction, there is still a great deal of clutter

Figure 1 BH-ASR system



(a)



(b)

Notes: (a) Out-field experiment; (b) data processing scheme

distributed around the edge of the stationary background objects, which is caused by unstable echoes from them. Compared with clutter, low-altitude target mapped in PPI radar image is an isolated gray spot with congregated degree in the relatively pure airspace. This spatial characteristic could be fully utilized to develop a new detection approach, say ECR detector.

Before the introduction of the ECR detector, two definitions should be given first. In the context of target detection, the detector is performed at the pixels of the subtracted image, including  $A$  false alarm pixels and  $B$  target pixels, thus we have many such binary tests, where the two possible outcomes are commonly denoted by  $H_0 = 0$  and  $H_1 = 1$ , corresponding to the null and positive hypotheses, respectively (McHugh *et al.*, 2009). The decision rule maps each of the observations into a decision of either  $H_0$  or  $H_1$ . To facilitate further discussion, the definitions of some variables are illustrated in Table I.

With these variables, we define two important evaluation criteria which are probability of detection ( $P_d$ ) and probability of false alarms ( $P_{fa}$ ):

$$P_d = T/B \quad (1)$$

$$P_{fa} = F/A \quad (2)$$

First, the subtracted image is binarized by the fixed-threshold approach, which is the simplest and most classical detector. The primary detection result  $\mathbf{B}_{FT}(i, j, k)$  is given:

$$\mathbf{B}_{FT}(i, j, k) = \begin{cases} 1 & \text{if } \mathbf{F}(i, j, k) > S_{FT} \\ 0 & \text{others} \end{cases}, \quad (3)$$

where  $\mathbf{F}(i, j, k)$  represents the intensity value of the  $(i, j)$  pixel in the  $k$ th foreground image after background subtraction, and  $S_{FT}$  is the fixed threshold. In this step, the threshold is usually set low enough to obtain a high  $P_d$  at the cost of an increase in  $P_{fa}$ . Subsequently, we could use the ECR detector to reject the clutters, reducing the  $P_{fa}$  to a low level. The rejection is done based on the result given by equation (3):

$$\mathbf{B}_{ECR}(i, j, k) = \begin{cases} 1 & \text{if } \mathbf{D}_{ECR}(i, j, k) < S_{ECR} \text{ and } \mathbf{B}_{FT}(i, j, k) = 1 \\ 0 & \text{others} \end{cases}. \quad (4)$$

where  $S_{ECR}$  is the edged clutter threshold. It is worth emphasizing that the ECR detector is exclusively applied to the pixels with  $\mathbf{B}_{FT}(i, j, k) = 1$ , which are the primary detection results in the foreground image. The inclusion of this condition could greatly reduce the computational cost. And, the  $\mathbf{D}_{ECR}(i, j, k)$  is calculated as below:

Table I Definitions of some variables

|                | True $H_0$ | True $H_1$ |
|----------------|------------|------------|
| Declared $H_0$ | $A-F$      | $B-T$      |
| Declared $H_1$ | $F$        | $T$        |
| Total          | $A$        | $B$        |

$$\mathbf{D}_{ECR}(i, j, k) = \frac{\sum_{m=-L_{out}/2}^{L_{out}/2} \sum_{n=-W_{out}/2}^{W_{out}/2} \mathbf{O}(i+m, j+n, k) - \sum_{m=-L_{in}/2}^{L_{in}/2} \sum_{n=-W_{in}/2}^{W_{in}/2} \mathbf{O}(i+m, j+n, k)}{W_{out} \cdot L_{out} - W_{in} \cdot L_{in}}, \quad (5)$$

where  $\mathbf{O}(i, j, k)$  represents the intensity value of the  $(i, j)$  pixel in the  $k$ th original image. The function gives the mean intensity value of the interesting area, which is the fringe part in Figure 2, where  $W_{in}$  and  $L_{in}$  are the width and length range of the inside region and  $W_{out}$  and  $L_{out}$  are that of the outside region. Here, we set the outside range to  $W_{out} = 2W_{in}$  and  $L_{out} = 2L_{in}$ . Obviously, the pixel surrounded by the background echoes is more likely to be labeled as clutter than the one with relatively pure neighbors.

### Compared algorithms

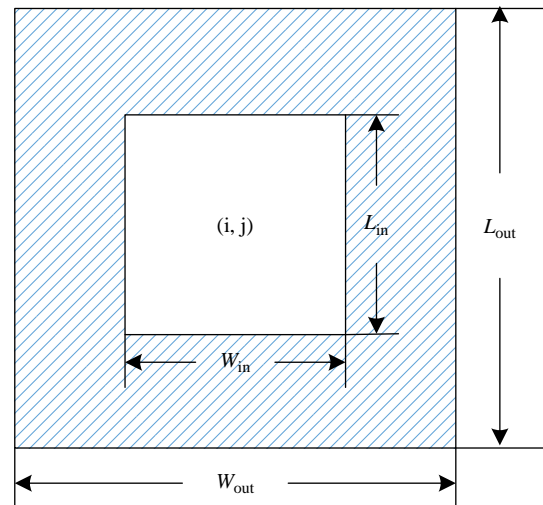
In our experiments, we compare the ECR algorithm with three other existing algorithms:

- 1 The fixed threshold, which is the simplest thresholding approach as equation (3), selects a global threshold value for the whole image.
- 2 The CA-CFAR processor (Gandhi *et al.*, 1988), which adaptively sets the threshold by estimating the mean level in a window of  $N$  range cells, is the optimum CFAR processor to maximize the detection probability. A target is declared to be present if the examined pixel exceeds the threshold  $S_{FT} \mathbf{D}_{CA}$ , where  $S_{FT}$  is a constant scale factor used to achieve a desired constant false alarm probability for a given window of size  $N$  and  $\mathbf{D}_{CA}$  is calculated as:

$$\mathbf{D}_{CA}(i, j, k) = \frac{1}{N} \left( \sum_{n=-N/2}^{-s} \mathbf{F}(i, j+n, k) + \sum_{n=s}^{N/2} \mathbf{F}(i, j+n, k) \right), \quad (6)$$

where  $s$  represents the size of the inside protected region. Then, the output of the CA-CFAR processor is:

Figure 2 ECR detector mask



$$\mathbf{B}_{CA}(i, j, k) = \begin{cases} 1 & \text{if } \mathbf{F}(i, j, k) > S_{FT} \cdot \mathbf{D}_{CA}(i, j, k) \\ 0 & \text{others} \end{cases} \quad (7)$$

- 3 The SO-CFAR processor is an alternative CFAR procedure, in which the threshold is obtained from the smallest sample of the reference window. The range samples are first ordered according to their magnitudes, and the statistic  $\mathbf{D}_{SO}(i, j, k)$  is taken to be the smallest sample of  $\{\mathbf{F}(i, j + n, k), n = [-N/2, \dots, -s, s, \dots, N/2]\}$ . So, the output of the SO-CFAR processor is:

$$\mathbf{B}_{SO}(i, j, k) = \begin{cases} 1 & \text{if } \mathbf{F}(i, j, k) > S_{FT} \cdot \mathbf{D}_{SO}(i, j, k) \\ 0 & \text{others} \end{cases}, \quad (8)$$

where  $S_{FT}$  is also used as the constant scale factor.

## Experimental results

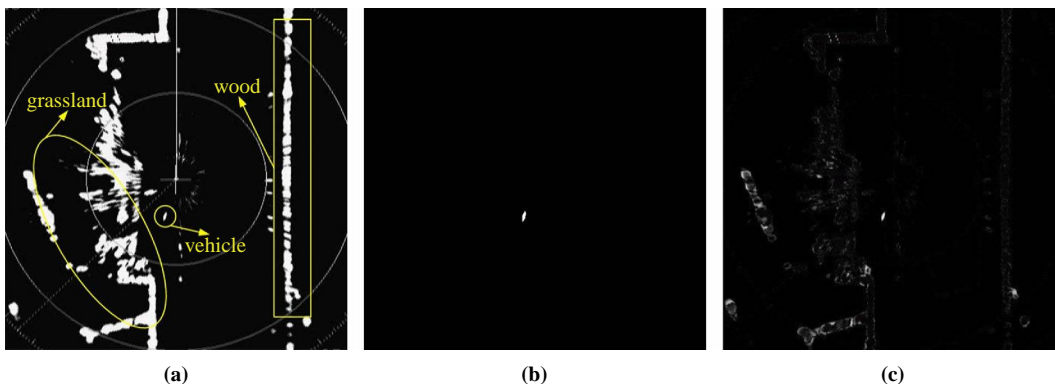
The above techniques have been applied to a sequence of PPI radar images: more specifically, one sequence of 24 frames tracking a vehicle, which is collected during the experiments at Nanyang Airport in October 2008. Note that the vehicle is not a target in low-altitude airspace in the strict sense; however, we take it as a substitute due to its easy controllability. The BH-ASR system was operated on the grassland beside the runway powered by a 24 V battery, when the vehicle target was running on the taxiway and the runway. The scanning period of the radar antenna is 2.5 s, so the capture card transforms the radar data received as function of range and azimuth into an x-y format every 2.5 s (24 frames per minute). The processed image is a  $456 \times 456$  pixel selection of the central part of the radar display. The grey value of each pixel is coded as an integer in the range of (0, 255). The spatial resolution of the radar image, which is the distance between two pixels, is set to 2 m.

Figure 3 shows one frame from the radar image sequence for test and its subtracted result. The original image is shown in Figure 3(a), the vehicle target is circled and the background objects including wood and grassland are also indicated. Most of the background objects are non-rigid and quasi-static (e.g. fluttering leaves and grass) that their radar echoes are

unstable and vary randomly on the edges. Figure 3(b) shows the manually generated ground-truth image following the procedures explained in Vicen-Bueno *et al.* (2011). After statistical study of the length and width of the vehicle based on the image sequence, the vehicle is modeled and its edges are labeled manually to approximate to the real shape of the target. The ideal ground-truth labels are binary, when each pixel of the target is indicated by 1 and the background by 0. This ideal image is needed for the estimations of  $P_d$  and  $P_{fa}$  in the designing of the detectors. Figure 3(c) shows the result after background subtraction. The background image is the mean output of the original image sequence. In the foreground image, the inside parts of the background objects are almost rejected whereas their marginal regions remain, whose intensities are sometimes even stronger than the real target. In the following experiments, the proposed ECR detector and the other compared detectors are applied on this foreground image. As analyzed in clutter rejection with spatial characteristics, the ECR detector is used for clutter rejection in addition to the fixed-threshold approach.

Figure 4 shows the probabilities of detection versus false alarms with the variation of the threshold, while Figure 5 shows the results of four algorithms with the  $P_d$  of 100 percent. It is encouraging that the inclusion of the ECR detector greatly improves the performance over the fixed-threshold approach and over the CFAR approaches. Thus, for a given  $P_d$ , the ECR detector results in a lower  $P_{fa}$  than the other procedures, while for a given  $P_{fa}$  it produces a much higher  $P_d$ . Since the probability density functions of the pixels under  $H_0$  and  $H_1$  are not known, numerical experiments with different thresholds are used to estimate both probabilities. Once a corresponding output image is obtained for a certain threshold, both probabilities are estimated by equations (1) and (2). For the comparative algorithms, the threshold  $S_{FT}$  is swept from 0 to 120 with the step of 2. We use the reference window with  $N = 24$  in equation (6) for the CA-CFAR processor with a protected window of the size of  $s = 8$ . For the SO-CFAR processor, we use the same size of the reference window as for CA-CFAR. Figure 5(a)-(c) provides the best detection results of the three comparative algorithms with the lowest number of false alarms when  $P_d$  is 100 percent; the fixed threshold is set to  $S_{FT} = 32$ . To reduce the false alarms without a decrease in  $P_d$ , we use the ECR detector mask with  $W_{in} = 16$  and  $L_{in} = 16$  to the result in Figure 5(a), and the clutter rejection threshold is set to  $S_{ECR} = 12$ . Clearly, when  $P_d$  remains at 1, the inclusion of the

**Figure 3** Radar image for test



**Notes:** (a) Original image; (b) ground-truth labels; (c) foreground image

**Figure 4** Performance comparison for target detection with the ECR detector on the data from Figure 3(c)

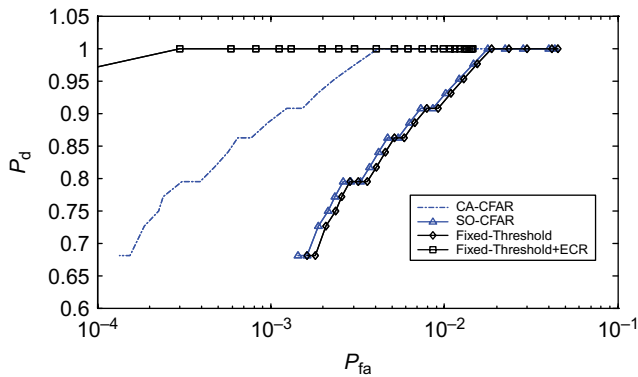
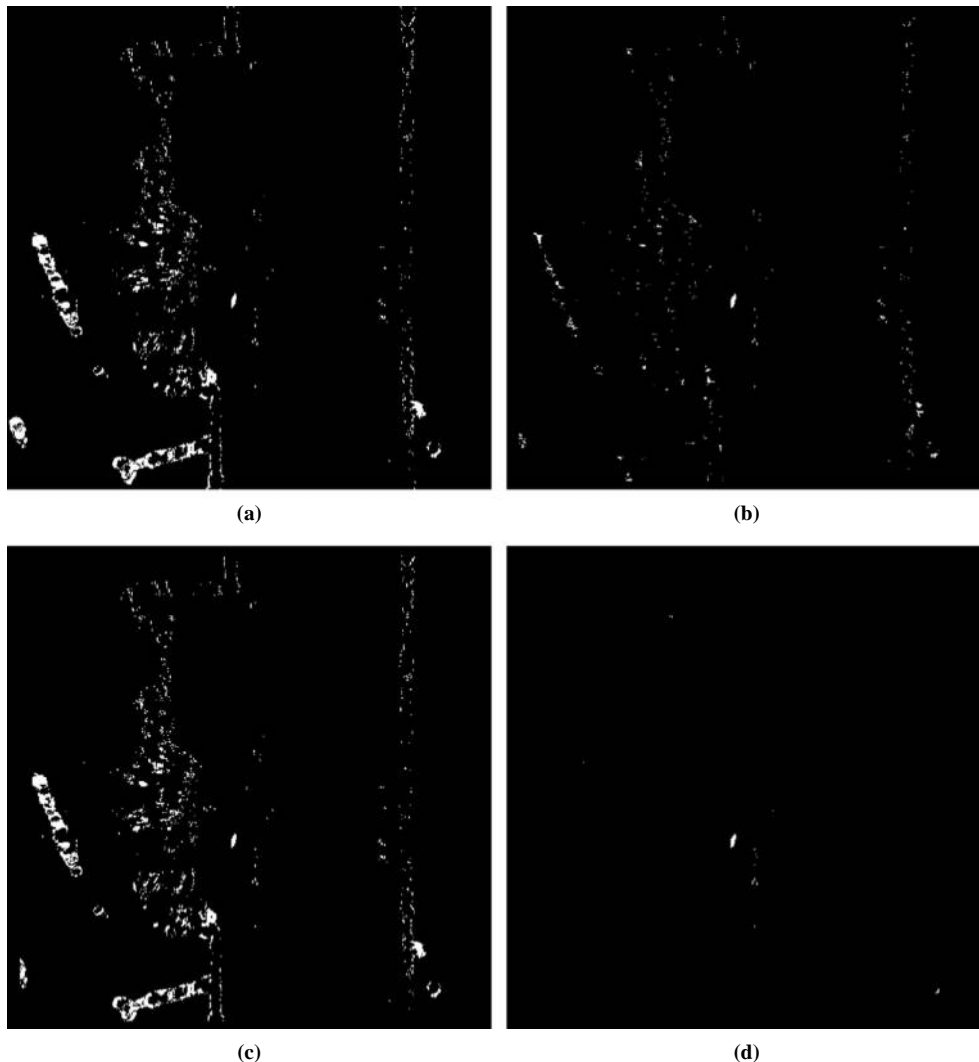


**Figure 5** Detection results with four algorithms where  $P_d = 1$



**Notes:** (a) Fixed-threshold ( $P_{fa} = 0.0174$ ); (b) CA-CFAR ( $P_{fa} = 0.0037$ ); (c) SO-CFAR ( $P_{fa} = 0.0165$ ); (d) fixed-threshold + ECR ( $P_{fa} = 0.0001$ )

ECR detector (Figure 5(d)) results in a significant decrease of false alarms compared to the other three algorithms (Figure 5(a)-(c)).

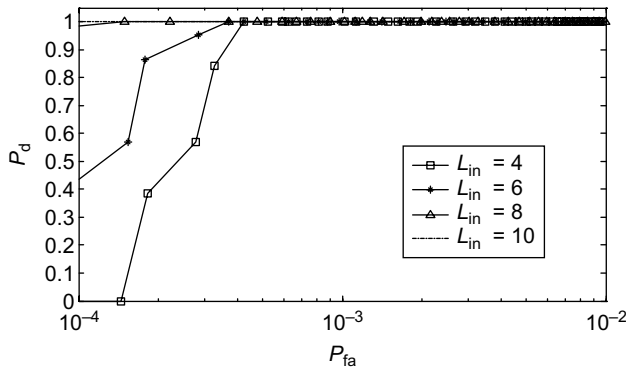
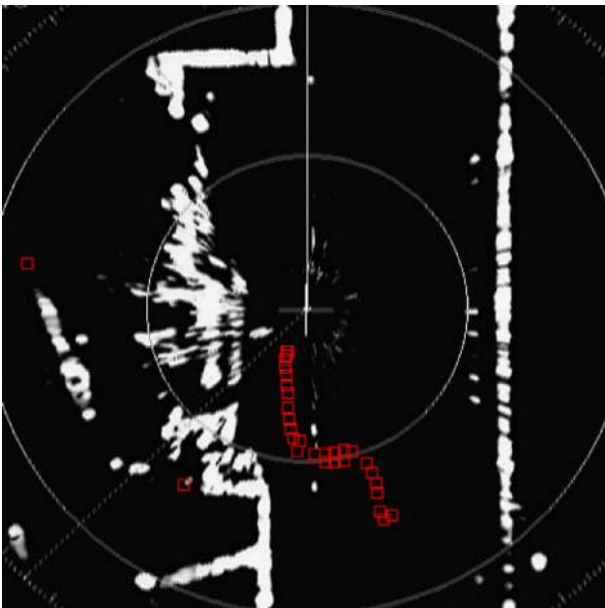
Efficiency of the detector is an important factor to the performance evaluation, so we record the computational cost of the four detectors for one image running in Matlab environment with 2.66 G CPU (Table II). The CFAR detectors are applied to all the pixels of the image, containing  $A + B$  pixels, while the ECR detector exclusively considers the detected pixels by fixed-threshold with 100 percent  $P_d$ , including a total of  $(A \cdot P_{fa} + B \cdot P_d)$  pixels. Since  $P_{fa}$  is usually at the magnitude of  $10^{-2}$  when  $P_d$  achieves 100 percent, the number of pixels concerned by the ECR detector accounts for merely 1 percent of those by CFAR detectors. Actually, the ECR detector remarkably improves the performance only with a slight increase in computational cost.

**Table II** Computational time cost (s)

| Fixed-threshold | CA-CFAR | SO-CFAR | Fixed-threshold + ECR |
|-----------------|---------|---------|-----------------------|
| 0.004           | 4.730   | 2.976   | 0.219                 |

The design of ECR detector mask shown in Figure 2 is important to achieve the best performance. Four parameters are considered for the detector mask:  $W_{in}$ ,  $L_{in}$ ,  $W_{out}$  and  $L_{out}$ . In this paper, we fix the scale between the outside and inside regions to two, and then only the values of  $W_{in}$  and  $L_{in}$  are varied. Figure 6 shows the performance achieved when  $W_{in}$  is fixed at 8 and the value of  $L_{in}$  changes. The  $P_{fa} - P_d$  pairs depend on the increase of  $S_{ECR}$  from 0 to 120. As observed, the selections of  $L_{in} = 8$  and 10 give the best results. This can be explained that the inside area of the mask with lower  $L_{in}$  cannot contain total information from the target and the pixels of the fringe area in Figure 2 should all belong to the background, removing the interferences from the target as much as possible.

After clutter rejection with the ECR detector, measurements are extracted from the binary image. Figure 7 shows the detection results of a vehicle from 24 frames of the sequence. All measurements are indicated by a square symbol at the

**Figure 6** Influence of the value of  $L_{in}$  on the ECR detector**Figure 7** Detection results of the sequence

current position and overlaid on the background image. From the figure, it is shown that the measurements include the target and small amount of false alarms. The measurements which constitute the trajectory belong to the target while the randomly distributed ones are false alarms. Note that sometimes there is more than one sign for the target in certain frames when it is divided by the range ring. Clearly, the ECR detector effectively realizes the surveillance of targets in low-altitude airspace with incoherent primary radar and reduces the number of clutters to the greatest degree.

## Conclusion

Clutter rejection technique for low-altitude surveillance system with incoherent primary radar is studied in this paper. The proposed ECR detector utilizes the spatial characteristics of the target in low-altitude airspace and the edged clutters to separate target from the PPI radar images. After analysis of the results present in this paper, several conclusions can be extracted. The most important one is that the ECR detector is suitable for clutter rejection in PPI radar image of low-altitude airspace, outperforming the fixed-threshold detector and the popular CFAR detectors. For a  $P_d = 1$ , the value of  $P_{fa}$  is reduced by approximate 0.017, 0.004 and 0.016 with the ECR detector, respectively, with respect to the detectors of fixed-threshold, CA-CFAR and SO-CFAR. Moreover, the computational time cost does not increase much in the ECR detector than the fixed-threshold detector.

For future work, the proposed ECR detector could be optimized by changing the size and shape of the detection mask according to different targets. It may also be interesting to test the generalization capability of the ECR detector for radar images collected in various low-altitude environments. For example, the situations when multiple targets are so closely spaced should be considered. The proposed algorithm could also be compared with other algorithms, such as the popular target detection algorithms for video surveillance:

- the visual background extractor (Barnich and Van, 2011); and
- the non-parametric background modeling algorithm (Elgammal *et al.*, 2000).

Otherwise, the target detection algorithm could be combined with the tracking algorithm in order to improve the results, which is the subject of further investigation.

## References

- Barnich, O. and Van, D.M. (2011), "ViBe: a universal background subtraction algorithm for video sequences", *IEEE Trans. Image Processing*, Vol. 20 No. 6, pp. 1709-1724.
- Elgammal, A., Harwood, D. and Davis, L. (2000), "Non-parametric model for background subtraction", *6th Proc. Eur. Conf. Computer Vision, Dublin, Ireland*, pp. 1-17.
- Hammoudi, Z. and Soltani, F. (2004), "Distributed CA-CFAR and OS-CFAR detection using fuzzy spaces and fuzzy fusion rules", *IEEE Proceedings, Radar, Sonar and Navigation*, Vol. 151 No. 3, pp. 135-142.
- He, Q., Lehmann, N.H., Blum, R.S. and Haimovich, A.M. (2005), "MIMO radar moving target detection in homogeneous clutter", *IEEE Trans. Aerosp. Electron. Syst.*, Vol. 46 No. 3, pp. 1290-1301.
- Li, Z.Z., Qi, L., Li, W., Jin, G. and Wei, M. (2009), "Track initiation for dim small moving infrared target based on

- spatial-temporal hypothesis testing”, *J. Infrared Milli. Terahz. Waves*, Vol. 30 No. 2, pp. 513-525.
- Lv, M.H., Yu, Q.Y. and Zhou, Q. (2009), “Applications of new ATM technology in low altitude space management”, *Communications Technology*, Vol. 42 No. 12, pp. 95-100.
- McHugh, J., Konrad, J., Saligrama, V. and Castanon, D. (2009), “Foreground-adaptive background subtraction”, *IEEE Signal Processing Letters*, Vol. 16 No. 5, pp. 390-393.
- Ning, H.S., Chen, W.S. and Li, J. (2010), “Bird-aircraft strike avoidance radar”, *IEEE Aerospace and Electronic Systems Magazine*, Vol. 25 No. 1, pp. 19-28.
- Vicen-Bueno, R., Carrasco-Alvarez, R., Rosa-Zurera, M. and Nieto-Borge, J.C. (2009), “Sea clutter reduction and target enhancement by neural networks in a marine radar system”, *Sensors*, Vol. 9 No. 3, pp. 1913-1936.
- Vicen-Bueno, R., Carrasco-Alvarez, R., Jarabo-Amores, M.P., Nieto-Borge, J.C. and Rosa-Zurera, M. (2011), “Ship detection by different data selection templates and multilayer perceptrons from incoherent maritime radar data”, *IET Radar Son. Nav.*, Vol. 5 No. 2, pp. 144-154.

### Further reading

- Buzzi, S., Lops, M. and Venturino, L. (2005), “Track-before-detect procedures for early detection of moving target from

- airborne radars”, *IEEE Trans. Aerosp. Electron. Syst.*, Vol. 41 No. 3, pp. 937-954.
- Gandhi, P. and Kassam, S. (2005), “Analysis of CFAR processors in nonhomogeneous background”, *IEEE Trans. Aerosp. Electron. Syst.*, Vol. 24 No. 4, pp. 427-445.

### About the authors

**Weishi Chen** was born in 1982 in Tianjin, China. He received his PhD degree from Beihang University in 2009. Now he is a Senior Engineer in Airport Research Institute, China Academy of Civil Aviation Science and Technology. His current research focuses on airport safety, low-altitude airspace surveillance and radar data processing.

**Huansheng Ning** was born in 1975 in Anhui province, China. He received the BS degree from Anhui University in 1996 and PhD degree in Beihang University in 2001. Now he is an Associate Professor in the School of Electronic and Information Engineering, Beihang University. His current research focuses on RFID, internet of things and their applications in aviation security. Huansheng Ning is the corresponding author and can be contacted at: ninghuansheng@buaa.edu.cn